九州大学学術情報リポジトリ
Kyushu University Institutional Repository

Experimental investigation on plugging performance of CO_2 microbubbles in porous media

Nam Nguyen Hai Le
Department of Earth Resources Engineering, Kyushu University

Sugai, Yuichi
Department of Earth Resources Engineering, Kyushu University

Vo-Thanh, Hung
School of Earth and Environmental Sciences, Seoul National University

Nguele, Ronald
Department of Earth Resources Engineering, Kyushu University

他

https://hdl.handle.net/2324/4785198

出版情報：Journal of Petroleum Science and Engineering. 211 (110187), 2022-04. Elsevier
バージョン：
権利関係：

KYUSHU UNIVERSITY

Experimental Investigation On Plugging Performance of CO_2 Microbubbles in Porous Media

Nam Nguyen Hai Le[a,b,c,*], Yuichi Sugai[a], Hung Vo-Thanh[d], Ronald Nguele[a], Ronald Ssebadduka[a], Ning Wei[e]

[a] Department of Earth Resources Engineering, Kyushu University, 744 Motooka, Nishi Ward, Fukuoka, Japan

[b] Faculty of Geology and Petroleum Engineering, Ho Chi Minh City University of Technology (HCMUT), 268 Ly Thuong Kiet Street, District 10, Ho Chi Minh City, Vietnam

[c] Vietnam National University Ho Chi Minh City, Linh Trung Ward, Thu Duc District, Ho Chi Minh City, Vietnam

[d] School of Earth and Environmental Sciences, Seoul National University, 1 Gwanak-ro, Gwanak-gu, Seoul, South Korea

[e] State Key Laboratory for Geomechanics and Geotechnical Engineering, Institute of Rock and Soil Mechanics, Chinese Academy of Sciences, Wuhan, Hubei Province, China

* Corresponding author: Nam Nguyen Hai Le (lnhnam@hcmut.edu.vn & le.nam.594@s.kyushu-u.ac.jp

Abstract

To further improve carbon dioxide enhanced oil recovery CO_2-EOR efficiency in heterogeneous reservoirs, the use of CO_2 microbubbles as a temporary blocking agent is attracting widespread interest due to their significant stability. This study aims to investigate the plugging performance of CO_2 microbubbles in both homogeneous and heterogeneous porous media through a series of sandpack experiments. First of all, CO_2 microbubble fluids were generated by stirring CO_2 gas diffused into polymer (Xanthan gum (XG)) and surfactant (Sodium dodecyl sulfate (SDS)) solution with different gas: liquid ratios. Then, CO_2 microbubbles fluids were injected into single-core and dual-core sandpack systems. The results show that the rheological behaviors of CO_2 microbubble fluids in this study were followed the Power-law model at room temperature. The apparent viscosity of CO_2 microbubble fluid increased as the gas: liquid ratio increased. CO_2 microbubbles could block pore throat due to the "Jamin effect" and increase the resistance in porous media. The blocking ability of CO_2 microbubbles reached an optimal value at the gas:liquid ratio of 20 % in the homogeneous porous media. Moreover, the selective pugging ability of CO_2 microbubbles in dual-core sandpack tests was significant. CO_2 microbubbles exhibited a good flow

control profile in the high permeability region and flexibility to flow over the pore constrictions in the low permeability region, leading to an ultimate fractional flow proportion (50%:50%) in the dual-core sandpack model with a permeability differential of 1.0:2.0 darcy. The fractional flow ratio was considerable compared with a polymer injection. At the higher heterogeneity of porous media (0.5:2.0 darcy), CO_2 microbubble fluid could still establish a good swept performance. This makes CO_2 microbubble fluid injection a promising candidate for heterogeneous reservoirs where conventional CO_2 flooding processes have limited ability. This finding would be helpful in developing the utilization of CO_2 microbubbles in EOR operation by better understanding their plugging mechanism in porous media.

Keywords

CO_2 microbubble, heterogeneous porous media, plugging ability, CO_2-Enhanced Oil Recovery, Single-core sandpack model, Dual-core sandpack model

43 **Graphical abstract**

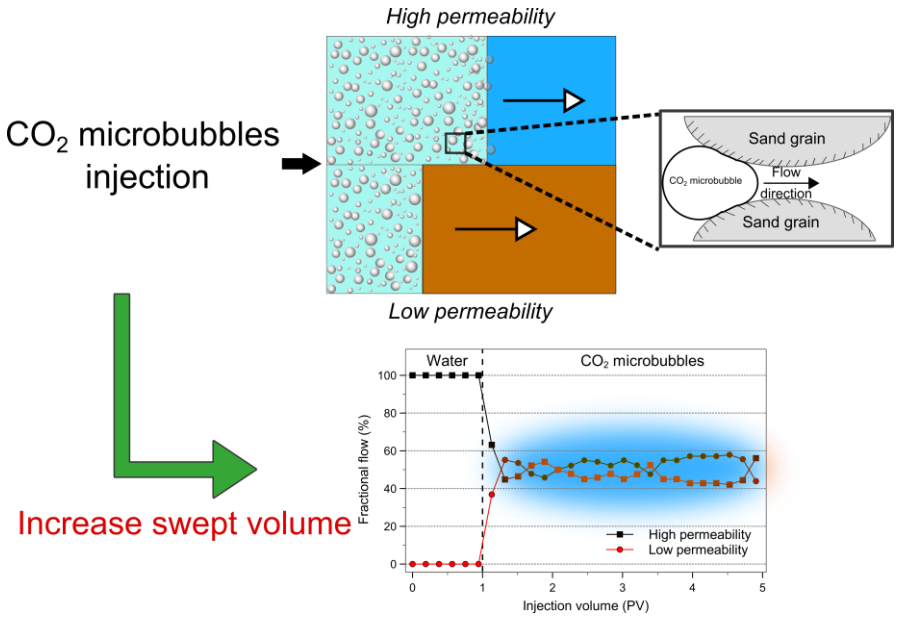

44

1 Introduction

With the increasing impact of global warming over the last decades, more carbon dioxide (CO_2) needs to be diminished to a sustainable level as a long-term consequence. Hence, carbon mitigation techniques have gained global attention as a potential method to reduce CO_2 emissions. At present, most research focuses on the topics of carbon capture and storage (CCS) and carbon capture, utilization and storage (CCUS). CCS comprises capturing CO_2 generated by burning fossil fuels for energy and sequestering it underground permanently (Dejam and Hassanzadeh, 2018a, 2018b; Vo Thanh et al., 2020a, 2019; Vo Thanh and Lee, 2021).

While in the CCUS, captured CO_2 is effectively utilized in industrial processes (Han et al., 2019). One of the primary techniques of CCUS is the utilization of CO_2 for enhancing oil recovery (CO_2-EOR)(Mohagheghian et al., 2019; Vo Thanh et al., 2020b). Additional oil could be extracted by utilizing large amounts of CO_2. Moreover, depleted oil and gas reservoirs can be potential formations for CO_2 storage (Bachu, 2016). From an industrial ecology perspective (Meylan et al., 2015), CO_2-EOR is reasonable and sustainable to control global CO_2 emissions.

In general, the implementation of CO_2 in EOR consists of miscible flooding and immiscible flooding. However, their performance is not always achievable due to several drawbacks, such as density effect, gas channeling, and poor sweep efficiency in heterogeneous porous media (Zhang et al., 2019). All those challenges lead to limit the effectiveness of CO_2-EOR and raise the additional cost. Therefore, how to enhance the efficiency of CO_2-EOR in heterogeneous formation by effectively blocking high permeable zone is an essential task.

For this, CO_2 foam is often considered to improve mobility control during CO_2-EOR operation by increasing gas viscosity and redirecting fluid to low permeable areas (Du et al., 2020, 2018; Yang et al., 2019). However, the foam becomes unstable under harsh environments. Therefore, the stability of foam is a challenge for this application in EOR (Razavi et al., 2020). Recently, microbubbles have received special attention in several fields of industry (Molaei and Waters, 2015). With a unique structure, microbubbles can remain stable under a harsh environment longer than conventional foam.

The microbubbles (10-100 μm) were first reported as colloidal gas aphrons (CGAs) by (Sebba, 1987). Wang et al. , (2001) applied CGAs to separate the heavy metal elements from the aqueous solution in mineral processing. They found that CGAs could have an outstanding performance in

the flotation of CuO at specific operating conditions. Waters et al., (2008) evaluated the efficiency of the CGAs flotation system in separating CuO from SiO_2. The results revealed that CGAs utilization increased CuO recovery significantly compared with previous methods.

Hashim and Sen Gupta, (1998) recommend using CGAs in recovering cellulosic pulp from contaminated effluent. Bjorndalen et al. (2009) pointed out that CGAs fluid can successfully block the micromodel. The oil-based CGAs drilling fluid was examined by Shivhare and Kuru (2014). They reported that the aphrons exhibit a good plugging performance in porous media and restrict formation damage due to fluid invasion. Bjorndalen et al. (2014) conducted flow tests using CGAs fluid prepared by polymer and surfactant.

It was inferred that CGAs fluid could effectively block the water-wet porous media. Pasdar et al. (2019) studied the fluid invasion control ability of CGAs based fluid using a micromodel system. They found that fluid invasion through fracture can be decreased significantly by injecting CGAs fluid. The CGA flow properties in porous media were also investigated using a modeling approach. Alizadeh and Khamehchi (2015) developed a mathematical model to predict the stability of microbubbles in drilling fluid in operational conditions of a gas well.

Alizadeh and Khamehchi (2017) also presented a mathematical model to analyze the transportation of microbubbles in porous media. They thought that the invasion of microbubble fluid in porous media is influenced by the ratio of bubble diameter to grain size. Several studies found remarkable stability of the microbubbles compared with conventional foams (Bjorndalen and Kuru, 2008; Fred Growcock, 2004; Pasdar et al., 2018a, 2018b). To date, some researchers have experimentally studied the flow of CGAs in porous media.

CO_2 microbubbles have been described as a spherical CO_2 gaseous core with a multilayer surfactant and viscous liquid covering. The inner layer is between the gas core and liquid layer, and the outer double-layer of surfactant play is likely a barrier against the bulk liquid. The shell of microbubbles has the advantage of diminishing the gas transfer from the inside core to the bulk phase. Thus, its structure could provide lower gas diffusivity and higher stability than conventional foam, which merely consists of a gas sphere and a surfactant layer (Telmadarreie et al., 2016).

Through a flooding study in the heterogeneous model, Telmadarreie et al. (2016) examined the use of CO_2 microbubbles to improve heavy oil recovery. The authors observed that CO_2 microbubbles could divert fluid flow to the low permeable zone by blocking the fracture, thereby

increasing sweep volume. Natawijaya et al., (2020) studied the efficiency of CO_2 microbubbles for EOR in a parallel sandpack model. Their results showed that an incremental oil recovery could be achieved due to a high sweep volume in the low permeability sandpack. **Fig. 1** illustrates the general sketch of CO2 gas injection challenges in heterogeneous reservoirs as mentioned above. Meanwhile, CO_2 microbubbles can be considered to have more potential than conventional methods due to being flexible and eco-friendly for CO_2-EOR and storage projects.

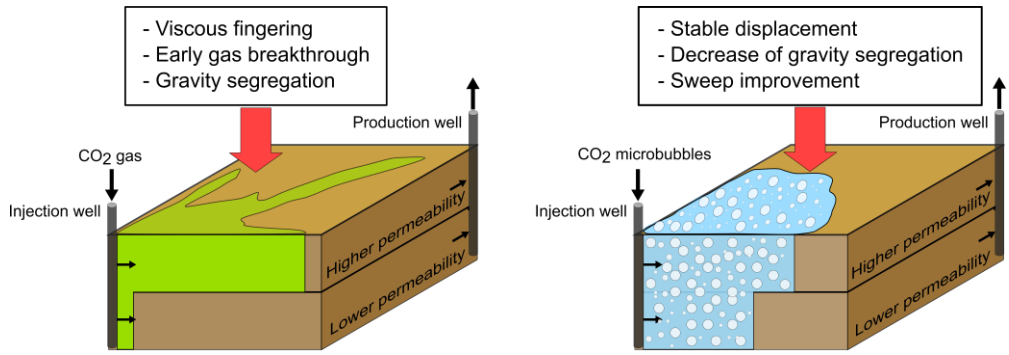

(a) CO_2 gas injection (b) CO_2 microbubble fluid injection

Fig. 1 The general sketch of the problem in this study.

Several experimental studies have demonstrated that microbubbles can be employed as a temporary blocking agent. However, few scholars have systematically investigated factors that affect the plugging ability of CO_2 microbubbles in homogeneous and heterogeneous porous media. Therefore, the objective of this paper is to obtain a better knowledge of flow restriction caused by CO_2 microbubbles in porous media. Bubble size distribution, stability, and rheological behavior of CO_2 microbubble fluids were thoroughly investigated. Besides, we conducted the sandpack flooding experiment to examine the plugging characteristic of CO_2 microbubbles. The pressure drop along the single sandpack model was recorded to evaluate the blockage efficiency for different gas: liquid ratio of CO_2 microbubble fluids, sand pack permeabilities and injection flow rates. Furthermore, the fractional volumes produced from dual-core sandpack models (simulated heterogeneous formations) were collected to analyze the swept improvement of CO_2 microbubbles. Thus, the finding of this work would propose some novel findings insight into the CO_2 microbubbles mechanism to recommend these fluids as the promising option for CO_2-EOR in the decade of energy transitions toward a carbon-neutral society worldwide.

This article is structured as follows: First, the materials and methods are described in Section 2.

Next, Section 3 presents the results obtained in this study. Eventually, some significant findings of this work are summarized in Section 4.

2 Materials and Methods

2.1 Materials

The chemicals used in this study include biopolymer Xanthan Gum (XG) and anionic surfactant sodium đoecyl sulfate (SDS, purity ≥ 98%), which were purchased from Junsei Chemical, Japan. CO_2 was supplied by a domestic company with a purity of 99.9%. Deionized water was used to make the base solutions with specific chemicals concentrations. These components are successfully applied in previous studies and provide good generating microbubbles performance(Arabloo and Pordel Shahri, 2014; Tabzar et al., 2015).

Silica sands with various meshes of 40-60 (250-400 μm), 60-70 (212-250 μm), and 100-170 (90-150 μm) were used for preparing the different permeability sandpacks.

2.2 Experimental Setup

Fig. 2 shows the sketch of sandpack flooding apparatus. The description of experimental procedures is highlighted below.

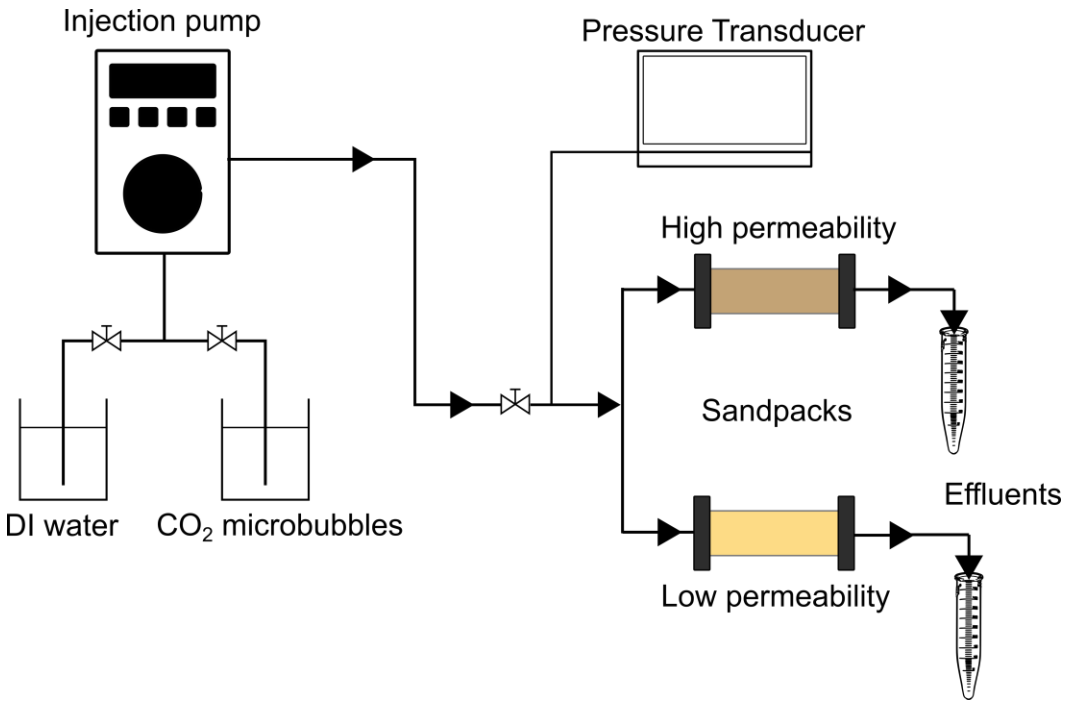

Fig. 2. Diagram of the experimental setup for CO_2 microbubble fluid flow in sandpacks.

The setup can conduct both single-core sandpack and parallel dual-core sandpack flow tests according to the plan of the experiment. An injection pump (PCS Pump SP-21) is used to inject fluid into the sandpacks at a specific flow rate. Two containers are used for holding DI water, and pre-generated CO_2 microbubbles fluid. The pressure change over the sandpack is measured using a pressure transducer (GC31-364, Nagano Keiki Co. Ltd., Japan) connected to the computer. The sandpacks have a diameter of 25 mm, and a length of 65 mm. The effluents are collected by the graduated glass tubes.

2.3 Experimental Methods

2.3.1 CO_2 microbubble fluids preparation

The base fluid was prepared by dissolving an amount of XG polymer (5000 mg/L), SDS surfactant (3000 mg/L) in 100 mL DI water using a magnetic stirrer (1000 rpm for 120 min). The base solution was transferred into a 200 ml container, and CO_2 was passed into the base fluid through a diffuser at a 20 ml/min gas flow rate using a flow regulator. The dispersion was homogenized at 8000 rpm for 4 min and gas: liquid ratio (ϕ) of CO_2 microbubble fluid ranging from 10% to 40% by adjusting the gas injection time. More details were presented by (Nguyen et al., 2021). For this action, the gaseous CO_2 entrained into the base fluid subsequently breaks into microscopic bubbles that are stabilized by polymer and surfactant molecules.

2.3.2 Characterization of CO_2 microbubble fluids

The CO_2 microbubbles were characterized by assessment of their bubble sizes, stabilities, and rheological properties.

The microscopic images of the CO_2 microbubbles were obtained using a microscope connected to a computer. The digital photographs were processed using an image processing software (ImageJ) to analyze the bubble size distribution. Around 300 microbubbles were examined in each sample to estimate the average diameter (D_{avg}), given by **Eq.1** :

$$D_{avg} = \frac{\sum_{i=1}^{N} D_i}{N} \quad (1)$$

where D_i (μm) is the diameter of the observed microbubbles and N is the total number of microbubbles in each sample.

The stability of CO_2 microbubbles was determined by visual monitoring. The fresh CO_2

microbubbles were transferred immediately to 10mL measuring cylinders for monitoring. Due to all sandpack flooding experiments being carried out within 2 hours, CO_2 microbubbles fluids must maintain their stabilities for more than 3 hours without phase separation.

The rheological properties of CO_2 microbubble fluids were studied using a viscometer (Brookfield DV-I Prime) at room temperature. Fluid samples were placed in the gap between a sample chamber and a rotating cylindrical spindle. The change of viscosity and shear stress versus various rotational speeds (from 0.5 to 100 rpm) were recorded. Four rheological models, such as Bingham plastic, Herschel-Bulkley, Power-law, and Casson, were presented to estimate the relationship between shear rate and shear stress to investigate the rheological characteristics of CO_2 microbubble fluids (Tabzar et al., 2015).

Bingham plastic model is presented by **Eq.2**:

$$\tau = \tau_0 + \eta\gamma, \tau_0 \geq 0, \eta > 0 \quad (2)$$

where τ: the shear stress, Pa; γ: the shear rate, s^{-1}- τ_0: the yield stress, Pa; η: plastic viscosity, Pa.s.

Herschel-Bulkley model is presented by **Eq.3**:

$$\tau = \tau_0 + K\gamma^n, \tau_0 \geq 0, K > 0, 0 < n < 1 \quad (3)$$

where τ: the shear stress, Pa; γ: the shear rate, s^{-1}; τ_0: the yield stress, Pa; K : the fluid consistency, n: the flow behavior index.

Power-law model is presented by **Eq.4**:

$$\tau = K\gamma^n, K > 0, 0 < n < 1 \quad (4)$$

where τ: the shear stress, Pa; γ: the shear rate, s^{-1}; K : the fluid consistency, n: the flow behavior index.

Casson model is presented by **Eq.5**:

$$\tau^{0.5} = \tau_0 + K\gamma^{0.5}, \tau_0 \geq 0, K > 0 \quad (5)$$

where τ: the shear stress, Pa; γ: the shear rate, s^{-1}; τ_0: the yield stress, Pa; K : the fluid consistency.

In addition, to represent the quality of fit, the coefficient of determination (R^2) and root mean square error (*RMSE*) were used.

Coefficient of determination is expressed by **Eq.6**:

$$R^2 = 1 - \frac{\sum(y_i - \hat{y}_i)^2}{\sum(y_i - \bar{y})^2} \quad (6)$$

where y_i: the experimental value, $\hat{y}_i$: the predicted value, $\bar{y}$: the average experimental value

Root Mean Square Error is expressed by **Eq.7**:

$$RMSE = \sqrt{\sum_{i=1}^{N} \frac{(\hat{y}_i - y_i)^2}{N}} \quad (7)$$

where y_i: the experimental value, $\hat{y}_i$: the predicted value, N: the number of data points

2.3.3 Preparation of sandpacks

The silica sands were cleaned and dried to remove impurities before use. Coarse sands (250-400 μm) were used to make high permeability sandpacks (2.0 darcy), whereas sands with 212-250 μm and 90-150 μm were used for medium permeability (1.0 darcy) and low permeability (0.5 darcy), respectively. Acrylic tubes were used as sandpack holders in this study. Each sandpack was shielded by rubber caps with contributor flowlines. Every single sandpack model was tightly packed with fresh sands mixing DI water. Then it was thoroughly saturated with DI water by continuous injecting at 1 mL/min to measure permeability and porosity. The porosity was then calculated by the mass balance. The permeability was obtained based on Darcy's law measurement.

2.3.4 CO_2 microbubble fluid flow tests

The following fluid flow experiments were performed to investigate the plugging ability of CO_2 microbubbles in porous media (see **Fig. 3**). A saturated single-tube sandpack was installed instead of the dual-core sandpack presented in **Fig. 2.**

Firstly, the DI water was injected into the sandpack at an adjusted flow rate to attain a steady injecting pressure. Then, 5 pore volume (PV) of CO_2 microbubbles was injected with the same flow rate. The pressure drop during the CO_2 microbubbles injection phase was recorded. By utilizing CO_2 microbubble fluid with various gas-liquid ratios, sandpack permeabilities, and injection flow rates, several single-core sandpack flow tests could be performed.

Dual-core sandpack test: Four heterogeneous dual-core sandpack models were conducted. First, two saturated sandpacks with different permeabilities were arranged parallel and connected to the flooding setup (see **Fig. 2**). Next, DI water was injected into the sandpack models (1mL/min) until

pressure drop along the sandpacks became stable. Then CO_2 microbubble fluid was injected at the same flow rate for 4 PV.

The effluents were collected by replacing the graduated measuring tube at regular intervals. The flows of effluents from the high and low permeability sandpack were collected to measure during injection processes. The pressure drop at these phases was also recorded.

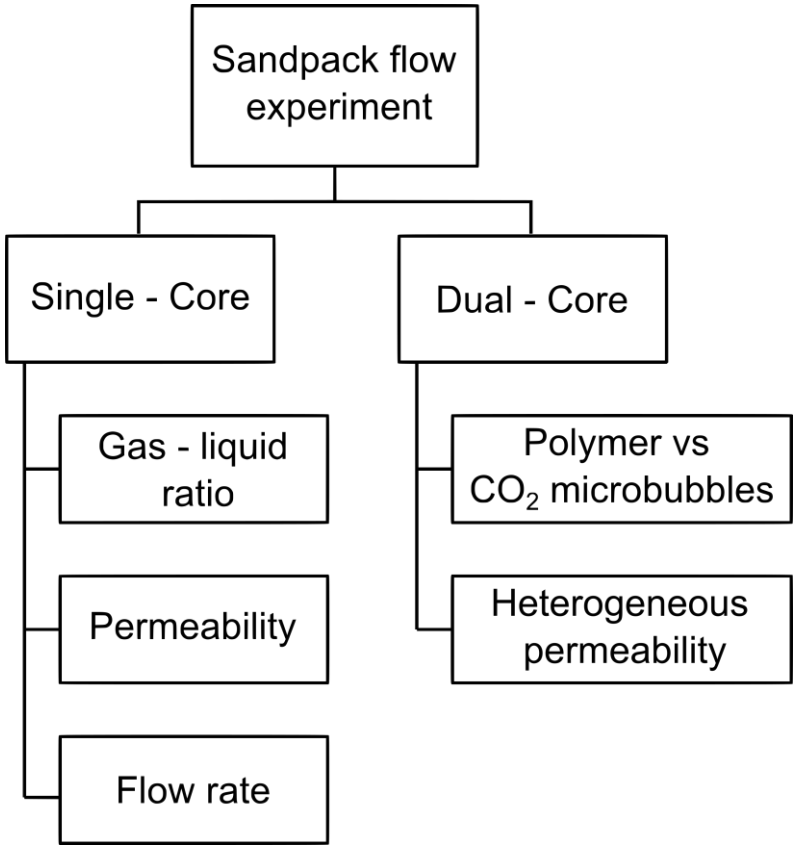

Fig. 3. Flowchart of the experimental procedure.

3 Results and Discussion

3.1 Bubble Size Distribution

Fig. 4 presents the micrographs of CO_2 microbubbles with different gas:liquid ratios.

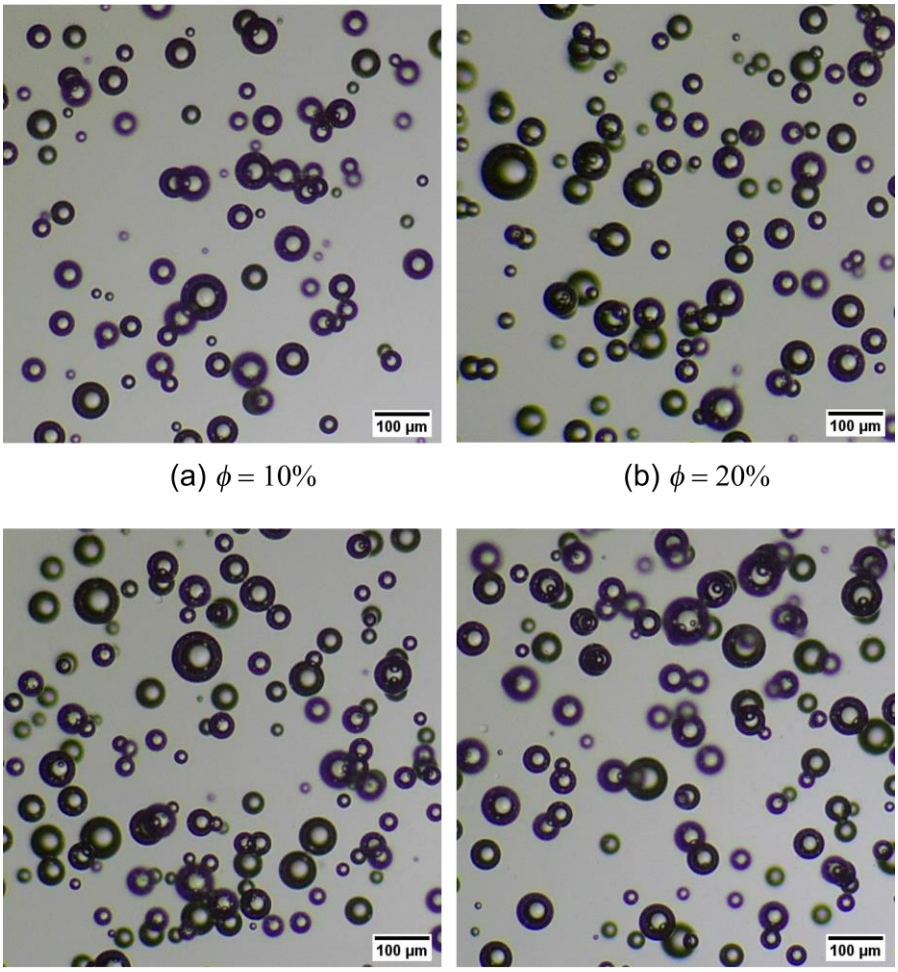

(a) $\phi = 10\%$ (b) $\phi = 20\%$

(c) $\phi = 30\%$ (d) $\phi = 40\%$

Fig. 4. Micrographs of CO_2 microbubbles with different gas:liquid ratios.

As illustrated, the CO_2 microbubble fluids with various gas-liquid ratios have a similar diameter distribution. The bubble size distribution and cumulative bubble size distribution of the four CO_2 microbubble fluids are illustrated in **Fig. 5**.

Bubble size ranges for the prepared fluids with gas-liquid ratios of 10 %, 20 %, 30 %, and 40 % are 11.1 µm – 87.6 µm, 12.82 µm - 106.8 µm, 9.3 µm - 93.1 µm, 8.7 µm - 99.9 µm, the median diameters (D_{50}) are 41.2 µm, 42.2 µm, 41.3 µm, and 41.2 µm, and the average diameters (D_{avg}) are 41.5 µm, 42.3 µm, 41.8 µm, and 42.8 µm, respectively. These results reveal that the prepared CO_2 microbubble fluids with different gas: liquid ratios had a comparatively similar bubble size distribution.

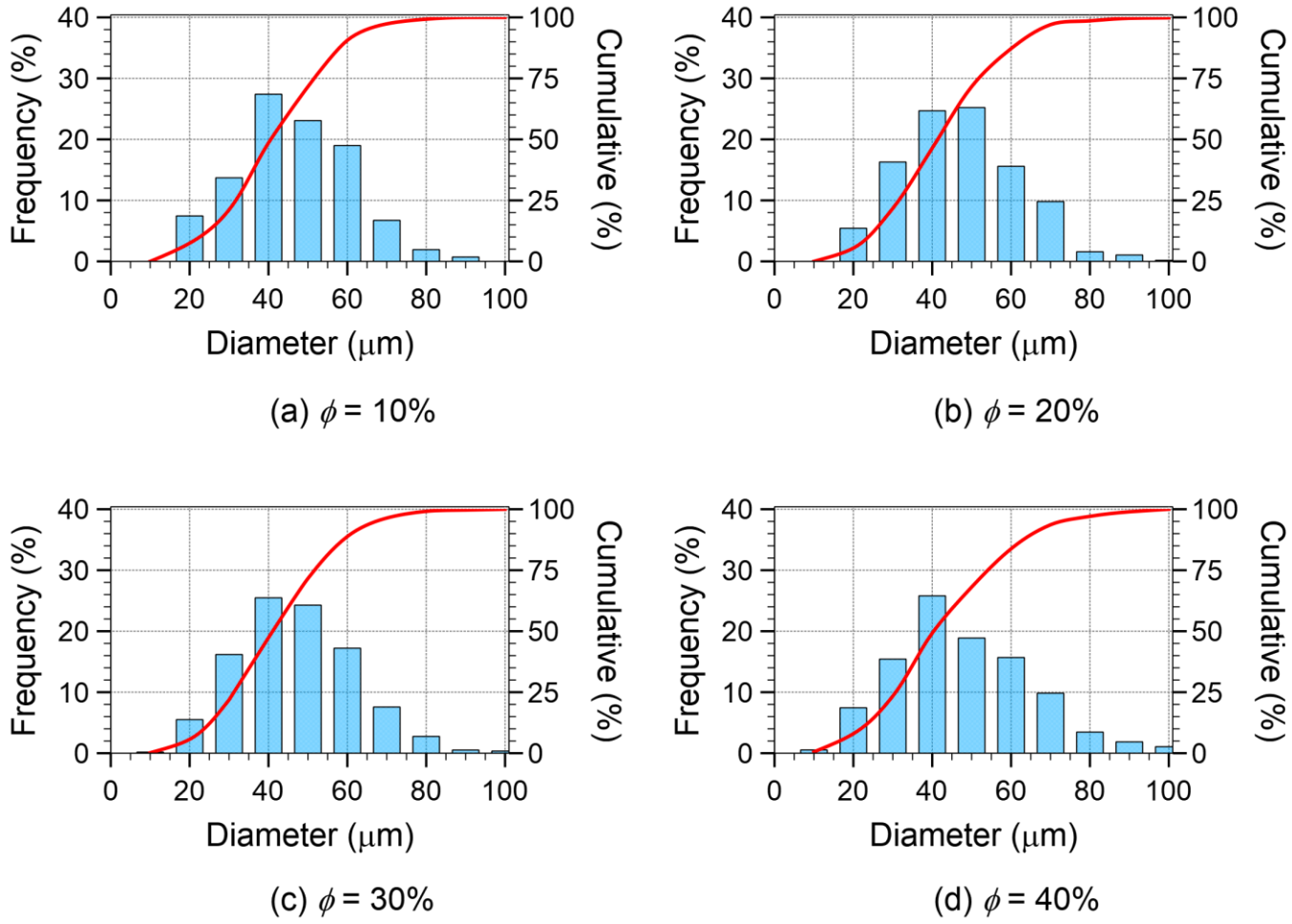

Fig. 5. Bubble size distribution of CO_2 microbubbles with different gas: liquid ratios.

3.2 CO_2 microbubbles stability

Fig. 6 depicts the images of the prepared CO_2 microbubble samples taken after homogenization as well as standing for three hours.

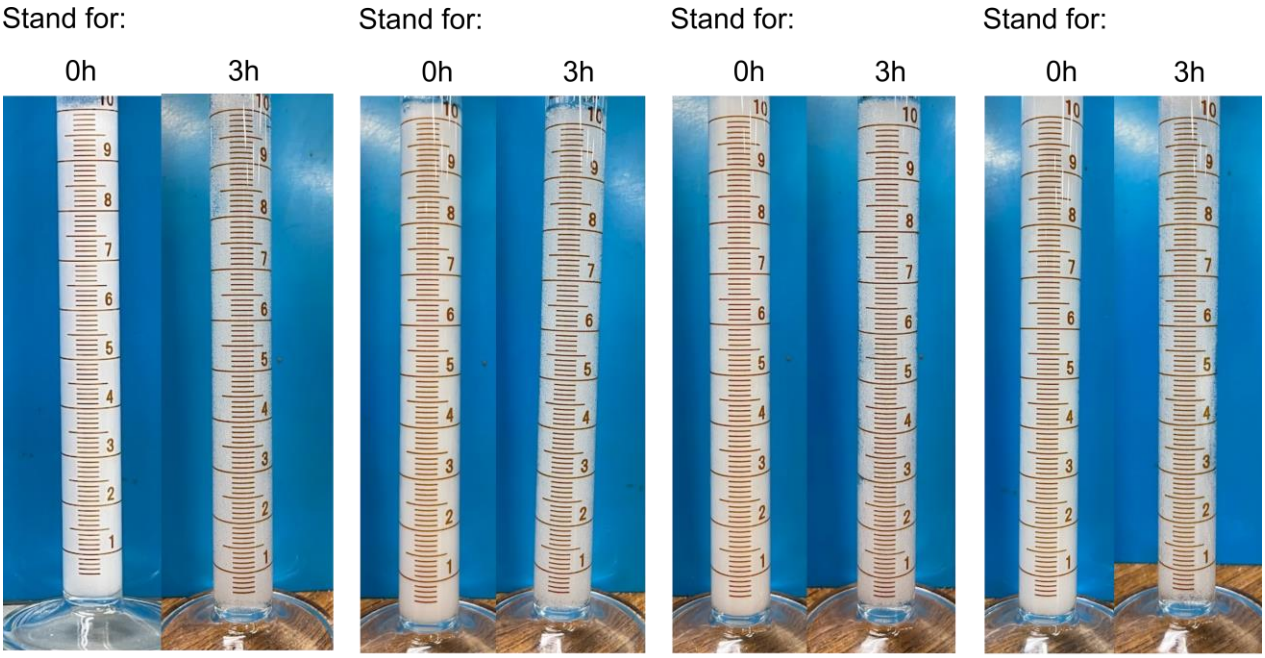

(a) $\phi = 10\%$ (b) $\phi = 20\%$ (c) $\phi = 30\%$ (d) $\phi = 40\%$

Fig. 6. Stability of CO_2 microbubble fluids at different gas: liquid ratios.

As one can see, CO_2 microbubble samples prepared with different gas:liquid ratios are all stable without phase separation after setting for three hours.

3.3 Rheological Properties of CO_2 Microbubbles Fluids

Table 1 presents the fitting results of four models for the experimental data.

Table 1. Rheological model's parameters of CO_2 microbubble fluids

Rheological Model	Parameter	ϕ = 10%	ϕ = 20%	ϕ = 30%	ϕ = 40%
Bingham-Plastic	τ_0	3.055359	3.310558	3.318006	3.392324
	η	0.1332	0.146327	0.147507	0.148665
Herschel-Bulkley	τ_0	-3.36999	-5.22701	-5.20284	-3.63214
	K	6.665809	8.810786	8.797225	7.295275
	n	0.109685	0.093332	0.093902	0.110998
Power-law	K	3.247139	3.518088	3.528496	3.609718
	n	0.201292	0.20424	0.20463	0.201009
Casson	τ_0	1.590445	1.653144	1.654649	1.67602
	K	0.188232	0.198566	0.199527	0.198729

Fig. 7 presents the corresponding statistical svalues (R^2 and *RMSE*) of these rheology models.

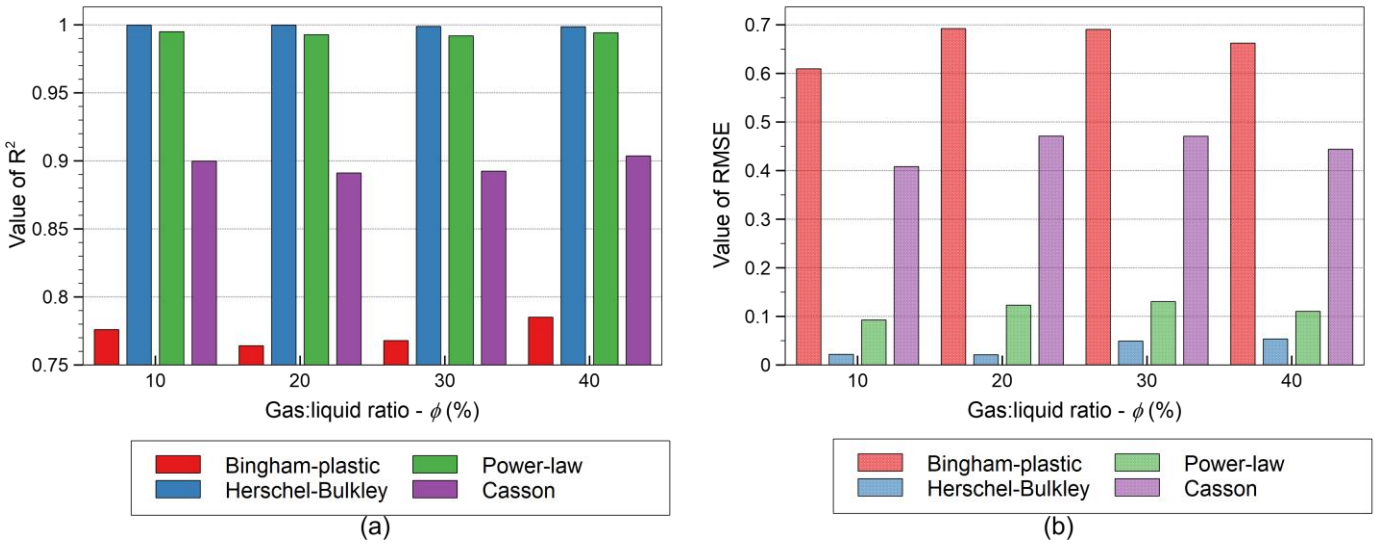

Fig. 7. Values of (a) R^2 and (b) *RMSE* of fitting models with CO_2 microbubble fluids at different gas: liquid ratios.

Among four rheology models, the Herschel-Bulkley model shows the highest R^2 values and the lowest *RMSE* values (**Fig. 7**); however, the yield point values (τ_0) are negative, as seen in **Table 1**. Therefore, they are unreasonable results when fitting the nonlinear regression of the shear rate and shear stress. Also, the Bingham-plastic model ranks as the worse performance (lowest R^2 values and highest *RMSE* values) compared with the other three models. Although the Power-law model did not achieve the high-value R^2 as the Herschel-Bulkley model, it produces more stable statistical values. In addition, previous studies also reported the same problem (Hassani and Ghazanfari, 2017; Zhu et al., 2020). As a result, the Power-law is the robust model for describing the rheology of CO_2 microbubble fluids since its good prediction (high quantity of R^2, low values of *RMSE*) and practical model parameters.

Fig. 8 presents the experimental shear stress data with fitting curves using the Power-law model versus the shear rate of CO_2 microbubble fluids at different gas: liquid ratios.

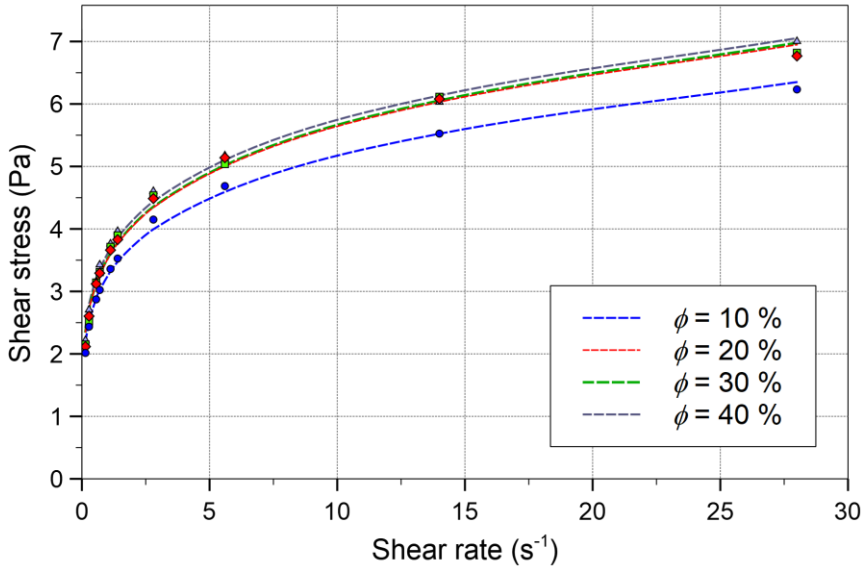

Fig. 8. Fitting cures of Power-law model for CO_2 microbubble fluids at different gas: liquid ratios.

The rheological parameters of the Power-law model are illustrated in **Table 1**. The consistency value, *K*, tends to increase with increasing ϕ. The flow index, n, is smaller than 1, which demonstrates that the CO_2 microbubble fluids in this study behave as a shear-thining fluid. The results also indicate that *n* remains the same regardless of the gas: liquid ratio (about 0.2). **Fig. 9** illustrates the variation of viscosities with rotational speeds of CO_2 microbubble fluids using the viscometer.

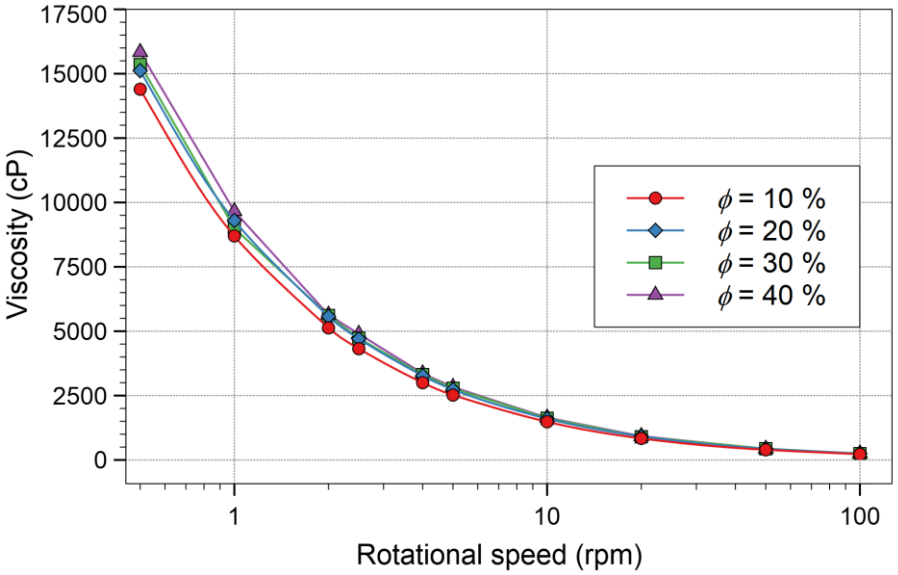

Fig. 9. The plot of viscosity vs. shear rate for CO_2 microbubble fluids at different gas: liquid ratios.

As the rotational speed increases, the viscosities of CO_2 microbubble fluids decrease rapidly. The fluid with a higher ratio of gas: liquid had a higher viscosity. The apparent viscosity (@100 rpm) of CO_2 microbubble fluids with gas: liquid ratios of 10, 20, 30, and 40 % are 222.6, 241.7, 243.5, and 250.1 cP, respectively.

3.4 CO_2 Microbubble Fluid Flow in Homogeneous Porous Media

Fig. 10 (a) and **(b)** show pictures of injected and produced CO_2 microbubble samples in one typical sanpack flow test.

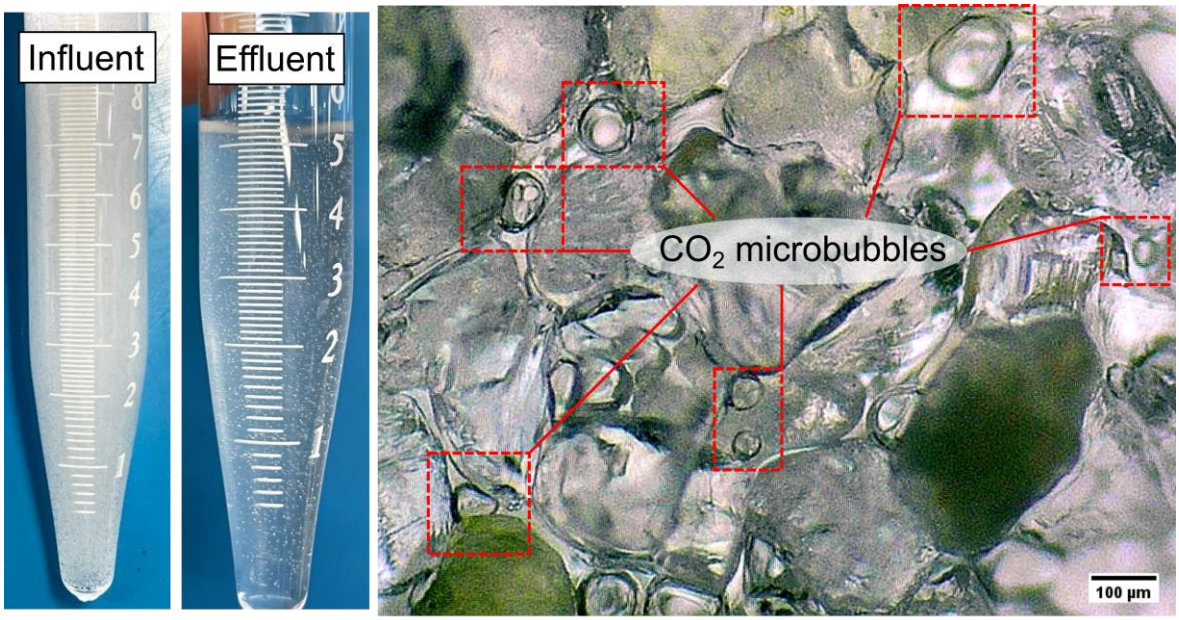

Fig. 10. (a) Injection CO_2 microbubble fluid; (b) Produced fluid from sandpack; (c) Microscopic image of CO_2 microbubbles in porous media.

As one can see, the number of CO_2 microbubbles in the effluent sample reduces considerably compared with the influent sample. **Fig. 10 (c)** also illustrates the microscopic image of CO_2 microbubbles distributed in porous media. It clearly demonstrates the pore throat blocking performance of CO_2 microbubbles to restrict the liquid flow in sandpack. **Fig. 11** presents a drawing of one CO_2 microbubble entering a pore constriction.

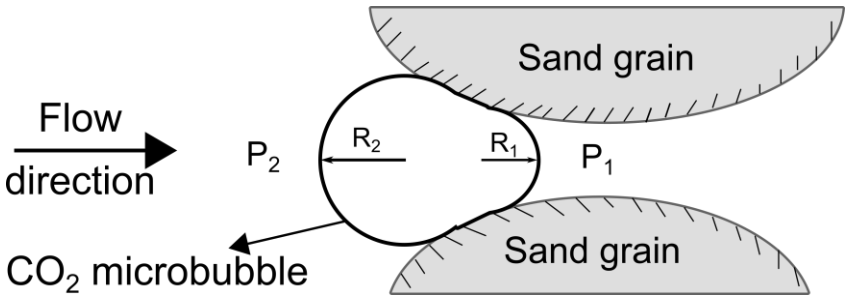

Fig. 11. Schematic representation of blockage mechanism as CO_2 microbubble enters the pore throat.

It will be under the action of capillary resistance force because of the "Jamin effect" (Wright, 1933), which is defined as the **Eq. (8)**.

$$\Delta P_c = P_2 - P_1 = 2\sigma\left(\frac{1}{R_1} - \frac{1}{R_2}\right) \tag{8}$$

where ΔP_c is the differential capillary pressure caused by the Jamin effect, P_1 and P_2 are pressure at the front and back of the microbubble. R_1 and R_2 are the front and back curvature radius when microbubble is deformed, respectively. σ is the interfacial tension

3.4.1 Effect of gas: liquid ratio

Fig. 12 presents the pressure drop by injecting CO_2 microbubble fluids with different ϕ of 10%, 20%, 30%, and 40% into 1.0 darcy permeability sandpacks (injection rate of 1 mL/min).

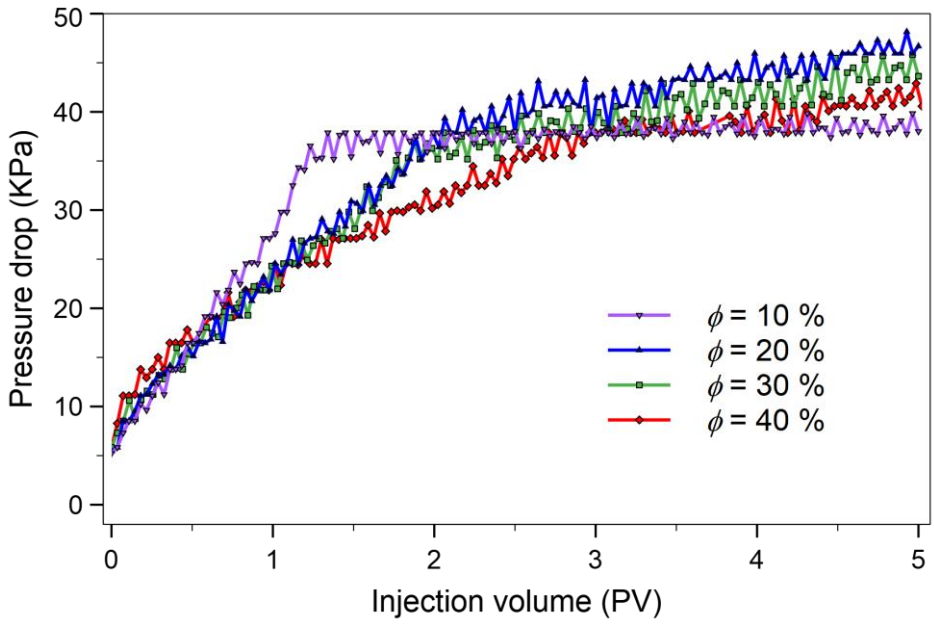

Fig. 12. Pressure drop changes during CO_2 microbubble fluid injecting as a function of gas: liquid ratios.

Generally, the pressure drop across the sandpacks significantly increased when CO_2 microbubble fluids with ϕ of 10%-40% were injected. This is because when CO_2 microbubbles go through the small pore throats, they need extra energy to overwhelm the differential pressure caused by the "Jamin effect" (Yang et al., 2020). As one can see, **Fig. 12** illustrates that CO_2 microbubble fluids reveal two types of flow regimes.

During the first stage, CO_2 microbubbles needed to travel through the whole system and temporarily block the large channel, which caused a sharp growth in the displacement pressure drop. After that, CO_2 microbubbles were flushed out of sandpack, so the injection pressure increased gradually and approached a stable state. By increasing ϕ, the concentration of microbubbles in the fluid was increased, resulting in a gradual increase in injection pressure.

When more microbubbles accumulate at the inlet of the sandpack, they cause fewer microbubbles to infiltrate into the system. Therefore, the fluids have higher microbubbles penetrate sandpack, resulting in more significant fluid flow restrictions because of the cumulative "Jamin effect". For the case of 10%, the pressure drop rose steeply in the initial stage and then reached a plateau of 38 KPa after injecting about 1.3 PV.

This indicated that the fluid with a low concentration of microbubbles could breakthrough faster than the other case and reduce the pore throat plugging efficiency. Preparing CO_2 microbubble fluid with a suitable ϕ value based on a correlation of bubble size, ϕ, and permeability could have an insightful meaning to the CO_2 microbubble application in EOR operation. By considering the injecting and plugging performance, the optimum gas: liquid ratio value is 20%.

3.4.2 Effect of sandpack permeability

Fig. 13 illustrates the impact of permeability on the CO_2 microbubble fluids injection. ϕ was kept at 20%, and the injection flow rate was set to 1 mL/min.

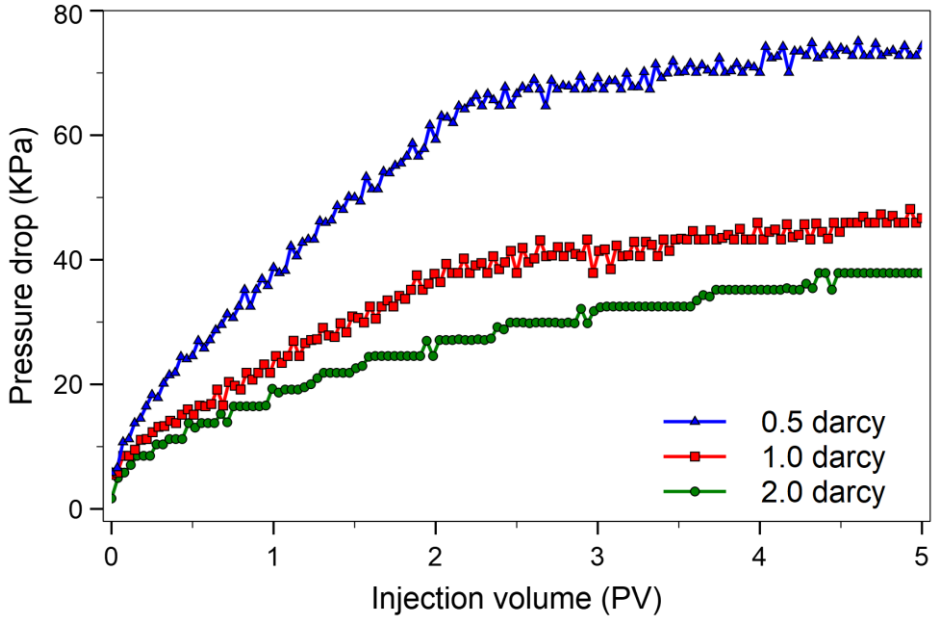

Fig. 13. Pressure drop changes during CO_2 microbubble fluid injecting into sandpack with different permeabilities.

As can be noticed, displacing pressure drops increase considerably as sanpack permeability decreases. The steady pressure drop increases from roughly 35 Kpa to 40 Kpa by reducing the permeability of the sandpack from 2.0 to 1.0 darcy. When the permeability of sandpack decreased to 0.5 darcy, the pressure drop increased quickly and reached a steady stage of 70 Kpa, almost twice larger than sandpack of 0.5 darcy.

These results indicate that CO_2 microbubbles are more easily transported in high permeability sandpacks. This result can be attributed to the fact that the pore throats in low permeability sandpacks have smaller diameters, causing higher capillary pressure. As a result, the CO_2 microbubbles could penetrate deeper into the high permeability sandpack. Therefore, in the case of heterogeneous porous media, CO_2 microbubbles could block large channels in high permeable zones and effectively divert the following flow into low permeable zones. This evidence is very suitable for fluvial channel reservoirs, whereas the depositional environment made the reservoir more complicated in terms of EOR application. Therefore, the plugging effect of CO_2 microbubbles could play an essential role in CO_2-EOR project in fluvial reservoirs.

3.4.3 Effect of the injection flow rate

Fig. 14 shows the pressure drop results for CO_2 microbubble fluid with ϕ = 20% in 1.0 darcy

sandpack at different injection rates (0.5, 1, and 2 mL/min).

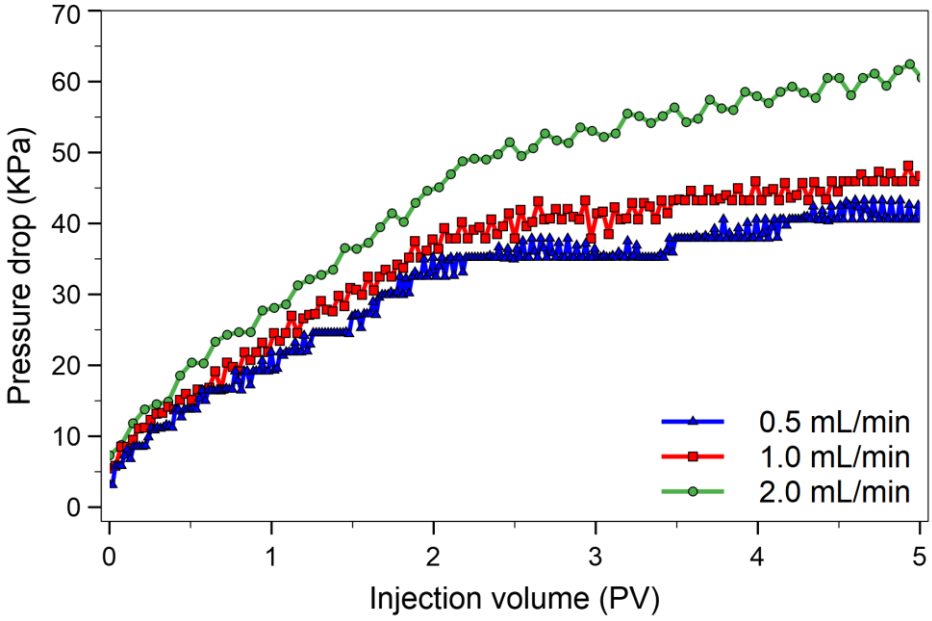

Fig. 14. Pressure drop changes during CO_2 microbubble fluid injecting with different flow rates.

As can be observed in **Fig. 14**, the pressure drop is more significant with higher injection flow rates. Besides, the stable pressure drop was reached at a higher volume of injected CO_2 microbubble fluid. The major cause of this phenomenon was that the trapped CO_2 microbubbles in porous media could be pushed and deformed when flowing through sandpack. Based on this mechanism, the CO_2 microbubbles can be transported through the pore throat to entrain into the following pores when the displacing pressure exceeds the resistance force resulting from the "Jamin effect".

Therefore, the increased injection pressure gradient due to the high injection rate would result in more and more CO_2 microbubbles overcoming their capillary resistance forces. This led to require more CO_2 microbubbles to be trapped in porous media. To consider CO_2 microbubbles for real field study, the injection rate is one of the critical operational control of the EOR project. The CO_2 microbubbles could replace the conventional CO_2 in the CCUS projects. Due to the favorable higher injection rate for the CCUS project, the higher injection rate injected inside the reservoirs that drove the higher amount of CO_2 could be stored in the hydrocarbon reservoirs. In addition, the CO_2 microbubbles-EOR has a dual function in the cleaner environment and improving the oil production in the EOR projects.

3.5 CO_2 Microbubble Fluid Flow in Heterogeneous Porous Media

As discussed previously, the appearance of CO_2 microbubbles could raise the flow resistance, hence improving sweep efficiency and changing the flow direction in porous media. Therefore, to further investigate the effectiveness of sweep efficiency enhancement, four heterogeneous dual-core sandpacks flow tests were conducted.

3.5.1 Plugging ability of CO_2 microbubbles in heterogeneous porous media

Fig. 15 (a) and **(b)** show the variations of fractional flows for injection of XG polymer with a concentration of 5000 mg/L and CO_2 microbubbles fluid (ϕ =20%) into dual-core sandpacks with the permeability differentials of 1.0: 2.0 darcy.

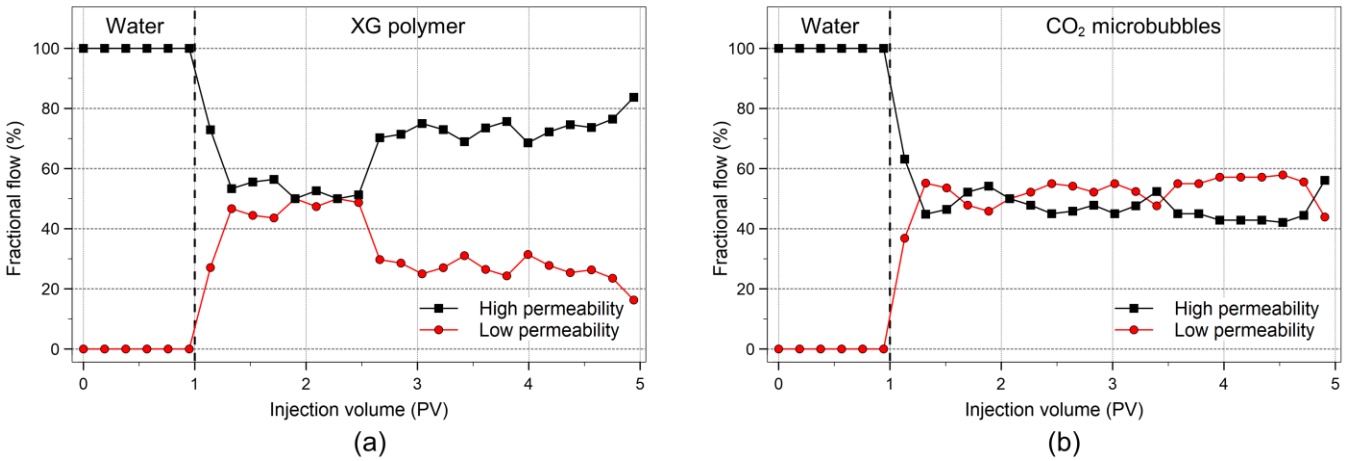

Fig. 15. Fractional flows of (a) CO_2 microbubble fluid with ϕ = 20% and (b) XG polymer solution (5000 mg/L) in dual-core sandpack (permeability ratio of 1.0:2.0 darcy).

The fluid was injected at 1 mL/min in this experiment. After 1 PV of water injection, the fractional flow ratios (low permeability: high permeability) are nearly 0:100 for two flow tests because of heterogeneity. After XG polymer injecting, the fractional flow ratio of the high and low permeability changes rapidly and approaches 50:50 after 1 PV of XG injection. As the XG polymer injection continues, the fractional flow of the low permeability decreases dramatically, and thereby the fractional flow ratio is about 35:65.

The difference is that when CO_2 microbubble was injected, the fractional flow ratio (low permeability: high permeability) altered from 0:100 to 55:45. The fractional flow of low permeability sandpack maintains at about 50% through the rest of the experiment

Fig. 16 compares the pressure drops of XG polymer and CO_2 microbubble fluid injection into dual-core sandpack of 1.0: 2.0 darcy.

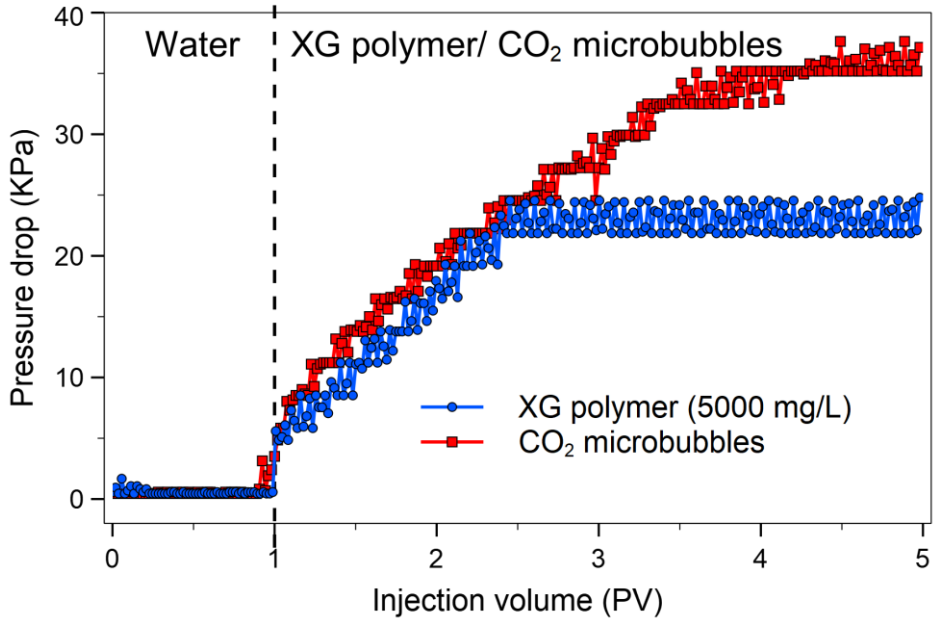

Fig. 16. Pressure drops of CO_2 microbubble fluid with ϕ = 20% and XG polymer solution (5000 mg/L) in dual-core sandpack (permeability ratio of 1.0:2.0 darcy).

As shown in **Fig. 16**, CO_2 microbubble injection leads to a higher displacing pressure drop than XG polymer injection. XG polymer reaches the flatten pressure drop at 2.5 PV while the CO_2 microbubble can maintain the pressure drop until the end of the injection process. This result demonstrates that the CO_2 microbubbles have a good plugging ability in heterogeneous porous media. Furthermore, it leads to an outstanding sweep improvement in low permeability sandpack. In this context, the unique structure of CO_2 microbubbles can block the pore constriction of the high permeable zone because of the "Jamin effect" and lead to flow diversion. On the other hand, the polymer increases the viscosity of the injecting solution cause improving flow resistance in porous media. As depicted in **Fig. 17**, the injected water preferentially passes into the sandpack with high permeability during the water flooding stage due to the formation heterogeneity.

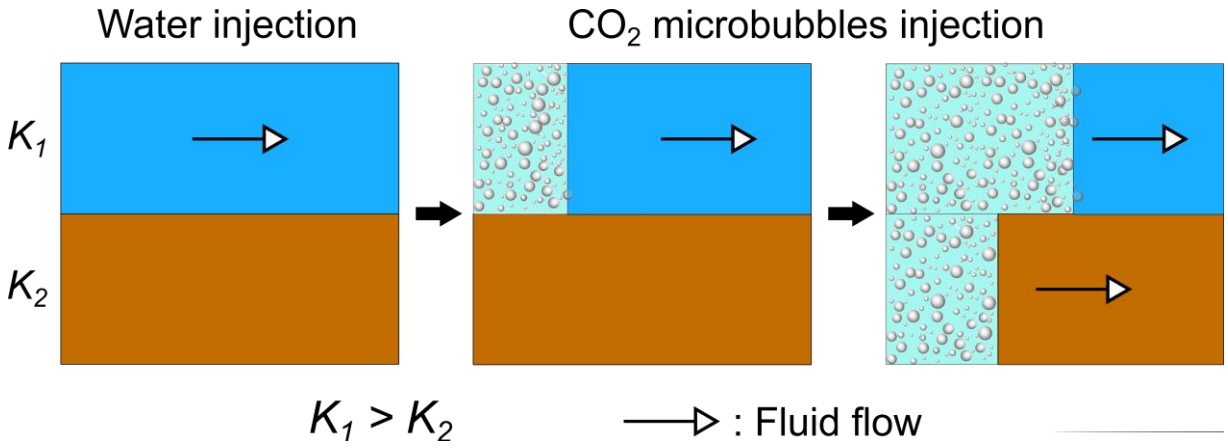

Fig. 17. Schematic illustration of the flow of CO_2 microbubble fluid in heterogeneous porous media.

Once CO_2 microbubble fluid is injected, they primarily enter the high permeability (K_1) sandpack and plug the pores. Therefore, the injected fluid could be diverted into the sandpack with low permeability (K_2), increasing sweep efficiency.

3.5.2 Sweep improvement of CO_2 microbubbles in dual-core sandpacks with different heterogeneities

Fig. 18 presents the changes in fractional flows for injection of CO_2 microbubble fluids with ϕ of 20% into dual-core sandpacks with different permeability ratios of 0.5:1.0 darcy and 0.5:2.0 darcy.

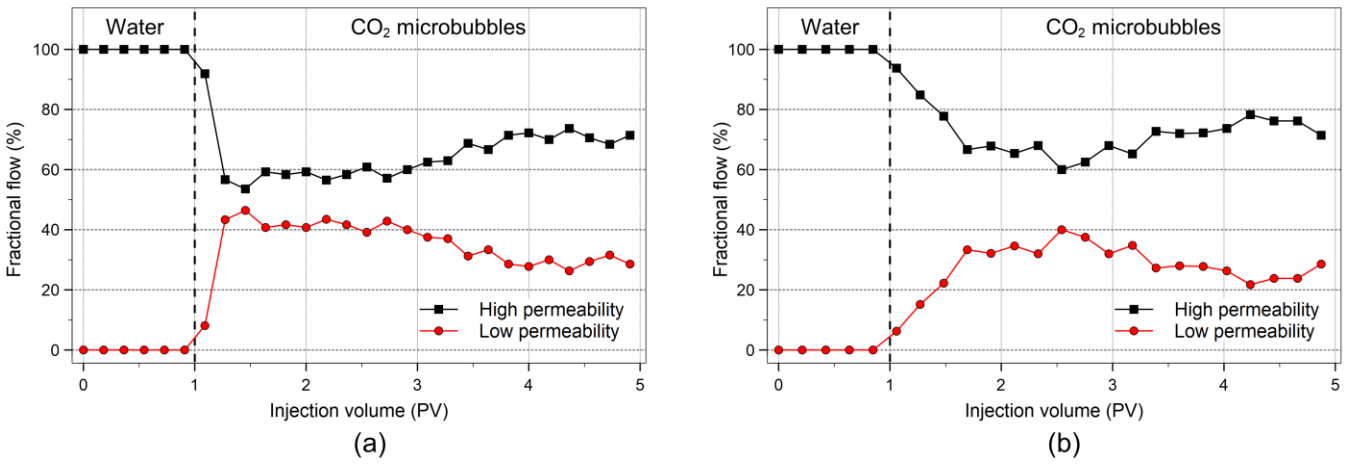

Fig. 18. Fractional flows of CO_2 microbubble fluid with ϕ = 20% in dual-core sandpacks with different permeability ratios: (a) 0.5:1.0 darcy; (b) 0.5:2.0 darcy.

The injection rate was set at 1 mL/min in this experiment. In the previous test, CO_2 microbubble fluid (ϕ =20%) exhibited good sweep during continuous injection into the dual-core sandpack of 0.5:1.0 darcy. As displayed in **Fig. 18 (a)**, by decreasing the permeability ratio of dual-core sandpacks to 0.5:1.0 darcy, the fractional flow is higher than 40% in the low permeability sandpack with the early CO_2 microbubble fluid injection.

As the injection is continued, the fractional flows in both sandpacks slightly fluctuate. Then, the fractional flow ratio (low permeability: high permeability) is maintained at about 30:70 throughout the rest. With a higher permeability differential of 0.5:2.0 darcy, the performance of CO_2 microbubbles in the dual-core sandpack was decreased. As CO_2 microbubble fluid injection starts, fractional flow ratio increases gradually (from 0:100 to 30:70) in low permeability sandpack, and then decreases to the low value, about 20:80.

As displayed in **Fig. 18 (b)**, by decreasing the permeability ratio of dual-core sandpacks to 0.5:1.0 darcy, the fractional flow is higher than 40% in the low permeability sandpack and lower than 60% in the high permeability sandpack with the early CO_2 microbubble fluid injection. As the injection is continued, the fractional flows in both sandpacks slightly fluctuate. However, the fractional flow ratio is maintained at about 30:70 throughout the rest.

The pressure drop results of this experiment are shown in **Fig. 19**.

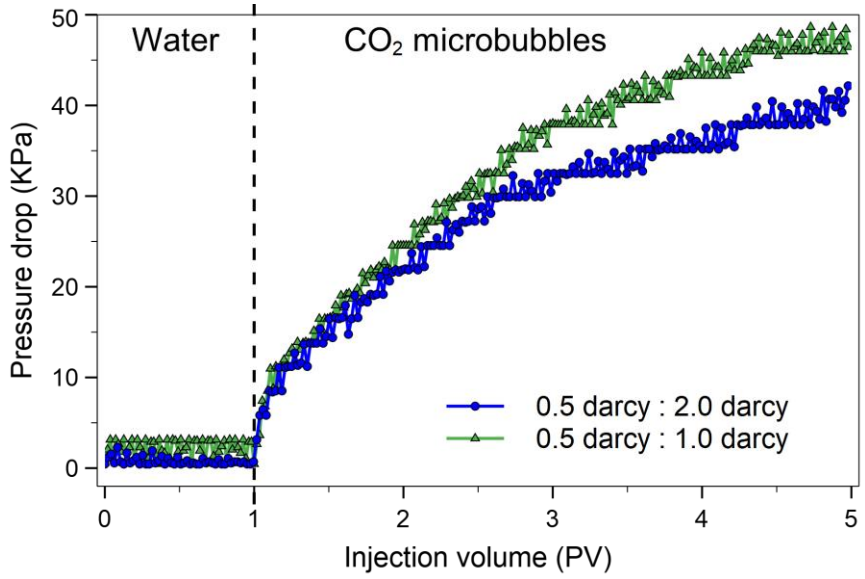

Fig. 19. Pressure drops of CO_2 microbubble fluid with ϕ = 20% in dual-core sandpacks with different permeability ratios: 0.5:1.0 darcy and 0.5:2.0 darcy.

The pressure drop in the case of 0.5:1.0 darcy is higher than that in the case of 0.5:2.0 darcy, indicating that the plugging ability of CO_2 microbubbles is more significant in a lower permeability ratio dual-core sandpack. However, the swept volume in low permeability sandpack showed significant improvement by injecting CO_2 microbubble fluid

4 Summary and Conclusions

In this paper, we discussed the advantages of CO_2 microbubbles for improving the efficiency of CO_2-EOR in heterogeneous formation. Several sandpack flooding experiments were systematically designed to investigate plugging characteristics of CO_2 microbubbles in porous media. Although unconsolidated formations were employed in this work, the dual-core sandpack model with different permeability gives an insight into the movement behavior of CO_2 microbubbles in heterogeneous porous media. The obtained results can be helpful in the upscaling process from the lab scale to the field scale. Based on the experimental results, the following conclusions could be drawn:

- The CO_2 microbubble fluids behave as shear-thinning fluid regardless of ϕ value. The rheological behavior of CO_2 microbubble fluid is described with the Power-law model due to its sufficient accuracy. Furthermore, the apparent viscosity of CO_2 microbubble fluids increases as the gas:liquid ratio increases.
- The gas:liquid ratio significantly affects the plugging ability of CO_2 microbubbles in porous media. The pressure drops first increased and then decreased with ϕ (range from 10 to 40%), peaking at ϕ = 20%. Because of "Jamin effect", CO_2 microbubbles can temporarily block pore constriction and resist flow in porous media. Therefore, the permeability of sandpack significantly influences the plugging performance of CO_2 microbubbles. Besides, the CO_2 microbubble fluid injection with a higher flow rate had a higher pressure drop over the sandpack.
- The dual-core sandpack flow tests indicate that CO_2 microbubbles have good properties for diverting flow and improving swept volume in the low permeable region of the heterogeneous formation. They can make a temporary plugging zone in the high permeability sandpack, and change the following fluid flow to the sandpack with low permeability. Although the sweep efficiency decreases by increasing the permeability

differential of the porous media, CO_2 microbubbles fluid is a good candidate for enhancing hydrocarbon recovery.

This work also has limitations on the effect of formation conditions on the sweep efficiency of CO_2 microbubbles. Therefore, the porous media saturated with oil under reservoir temperatures should be considered in further investigations. The rheological modeling of CO_2 microbubbles in porous media needs to be undertaken. Furthermore, to investigate the application of CO_2 microbubbles in field scale, numerical simulation is needed to match the laboratory core flooding data.

Acknowledgment

We would like to thank the support of time and facilities for this study from Kyushu University, Japan, and Ho Chi Minh City University of Technology (HCMUT), VNU-HCM, Vietnam.

Nomenclature

Abbreviations

CCS	Carbon capture and storage
CCUS	Carbon capture, utilization and storage
CGAs	Colloidal gas aphrons
CO_2	Carbon dioxide
EOR	Enhanced oil recovery
RPM	Round per minute
SDS	Sodium dodecyl sulfate
XG	Xanthan gum

Greek letters

ϕ	Gas:liquid ratio, %
γ	Shear rate, s^{-1}
η	Plastic viscosity, cP
σ	Interfacial tension between gas and liquid, mN/m
τ	Shear stress, Pa

τ_0	Yield stress, Pa

Subscripts

c	Capillary
avg	Average value
H	High permeability sandpack
L	Low permeability sandpack
i	Observed microbubble
1	Front of the microbubble
2	Back of the microbubble
50	Median value

Variables and parameters

ΔP_C	Differential capillary pressure
D_{50}	Median diameter, μm
D_{avg}	Average diameter, μm
D_i	Diameter of observed microbubble, μm
K_H	High permeability, darcy
K_L	Low permeability, darcy
n	Flow behavior index
N	Number of data points
P_1	Pressure at the front of the microbubble
P_2	Pressure at the back of the microbubble
PV	Pore volume, mL
R_1	Front curvature radius of the microbubble
R_2	Back curvature radius of the microbubble
R^2	Coefficient of determination
RMSE	Root mean square error
K	Fluid consistency

487

References

Alizadeh, A., Khamehchi, E., 2017. Mathematical modeling of the Colloidal Gas Aphron transport through porous medium using the filtration theory. J. Nat. Gas Sci. Eng. 44, 37–53. https://doi.org/10.1016/j.jngse.2017.04.013

Alizadeh, A., Khamehchi, E., 2015. Modeling of micro-bubble surfactant multi-layer drilling fluid stability based on single bubble behavior under pressure and temperature in a deviated gas well. J. Nat. Gas Sci. Eng. 26, 42–50. https://doi.org/10.1016/j.jngse.2015.05.027

Arabloo, M., Pordel Shahri, M., 2014. Experimental studies on stability and viscoplastic modeling of colloidal gas aphron (CGA) based drilling fluids. J. Pet. Sci. Eng. 113, 8–22. https://doi.org/10.1016/j.petrol.2013.12.002

Bachu, S., 2016. Identification of oil reservoirs suitable for CO2-EOR and CO2 storage (CCUS) using reserves databases, with application to Alberta, Canada. Int. J. Greenh. Gas Control 44, 152–165. https://doi.org/10.1016/j.ijggc.2015.11.013

Bjorndalen, H.N., Jossy, W.E., Alvarez, J.M., Kuru, E., 2014. A laboratory investigation of the factors controlling the filtration loss when drilling with colloidal gas aphron (CGA) fluids. J. Pet. Sci. Eng. 117, 1–7. https://doi.org/10.1016/j.petrol.2014.03.003

Bjorndalen, N., Alvarez, J., Jossy, E., Kuru, E., 2009. An Experimental Study of the Pore-Blocking Mechanisms of Aphron Drilling Fluids Using Micromodels. https://doi.org/10.2118/121417-ms

Bjorndalen, N., Kuru, E., 2008. Stability of microbubble-based drilling fluids under downhole conditions. J. Can. Pet. Technol. 47, 40–47. https://doi.org/10.2118/08-06-40

Dejam, M., Hassanzadeh, H., 2018a. Diffusive leakage of brine from aquifers during CO2 geological storage. Adv. Water Resour. 111, 36–57. https://doi.org/10.1016/j.advwatres.2017.10.029

Dejam, M., Hassanzadeh, H., 2018b. The role of natural fractures of finite double-porosity aquifers on diffusive leakage of brine during geological storage of CO2. Int. J. Greenh. Gas Control

78, 177–197. https://doi.org/10.1016/j.ijggc.2018.08.007

Du, D., Li, Y., Chao, K., Wang, C., Wang, D., 2018. Laboratory study of the Non-Newtonian behavior of supercritical CO2 foam flow in a straight tube. J. Pet. Sci. Eng. 164, 390–399. https://doi.org/10.1016/j.petrol.2018.01.069

Du, D., Zhang, X., Li, Y., Zhao, D., Wang, F., Sun, Z., 2020. Experimental study on rheological properties of nanoparticle-stabilized carbon dioxide foam. J. Nat. Gas Sci. Eng. 75, 103140. https://doi.org/10.1016/j.jngse.2019.103140

Fred Growcock, 2004. Enhanced Wellbore Stabilization and Reservoir Productivity with Aphron Drilling Fluid Technology. https://doi.org/10.2172/896513

Han, B., Wei, G., Zhu, R., Wu, W., Jiang, J.J., Feng, C., Dong, J.F., Hu, S.Y., Liu, R.Z., 2019. Utilization of carbon dioxide injection in BOF-RH steelmaking process. J. CO2 Util. 34, 53–62. https://doi.org/10.1016/j.jcou.2019.05.038

Hashim, M.A., Sen Gupta, B., 1998. The application of colloidal gas aphrons in the recovery of fine cellulose fibres from paper mill wastewater. Bioresour. Technol. 64, 199–204. https://doi.org/10.1016/S0960-8524(97)00169-7

Hassani, A.H., Ghazanfari, M.H., 2017. Journal of Natural Gas Science and Engineering Improvement of non-aqueous colloidal gas aphron-based drilling fl uids properties : Role of hydrophobic nanoparticles 42, 1–12.

Meylan, F.D., Moreau, V., Erkman, S., 2015. CO2 utilization in the perspective of industrial ecology, an overview. J. CO2 Util. 12, 101–108. https://doi.org/10.1016/j.jcou.2015.05.003

Mohagheghian, E., Hassanzadeh, H., Chen, Z., 2019. CO2 sequestration coupled with enhanced gas recovery in shale gas reservoirs. J. CO2 Util. 34, 646–655. https://doi.org/10.1016/j.jcou.2019.08.016

Molaei, A., Waters, K.E., 2015. Aphron applications - A review of recent and current research. Adv. Colloid Interface Sci. 216, 36–54. https://doi.org/10.1016/j.cis.2014.12.001

Natawijaya, M.A., Sugai, Y., Anggara, F., 2020. CO2 microbubble colloidal gas aphrons for EOR application: the generation using porous filter, diameter size analysis and gas blocking impact

on sweep efficiency. J. Pet. Explor. Prod. Technol. 10, 103–113. https://doi.org/10.1007/s13202-019-0680-3

Nguyen, N., Le, H., Sugai, Y., Nguele, R., Sreu, T., 2021. Bubble size distribution and stability of CO 2 microbubbles for enhanced oil recovery : effect of polymer , surfactant and salt concentrations. J. Dispers. Sci. Technol. 0, 1–11. https://doi.org/10.1080/01932691.2021.1974873

Pasdar, M., Kamari, E., Kazemzadeh, E., Ghazanfari, M.H., Soleymani, M., 2019. Investigating fluid invasion control by Colloidal Gas Aphron (CGA) based fluids in micromodel systems. J. Nat. Gas Sci. Eng. 66, 1–10. https://doi.org/10.1016/j.jngse.2019.03.020

Pasdar, M., Kazemzadeh, E., Kamari, E., Ghazanfari, M.H., Soleymani, M., 2018a. Monitoring the role of polymer and surfactant concentrations on bubble size distribution in colloidal gas aphron based fluids. Colloids Surfaces A Physicochem. Eng. Asp. 556, 93–98. https://doi.org/10.1016/j.colsurfa.2018.08.020

Pasdar, M., Kazemzadeh, E., Kamari, E., Ghazanfari, M.H., Soleymani, M., 2018b. Insight into the behavior of colloidal gas aphron (CGA) fluids at elevated pressures: An experimental study. Colloids Surfaces A Physicochem. Eng. Asp. 537, 250–258. https://doi.org/10.1016/j.colsurfa.2017.10.001

Razavi, S.M.H., Shahmardan, M.M., Nazari, M., Norouzi, M., 2020. Experimental study of the effects of surfactant material and hydrocarbon agent on foam stability with the approach of enhanced oil recovery. Colloids Surfaces A Physicochem. Eng. Asp. 585, 124047. https://doi.org/10.1016/j.colsurfa.2019.124047

Sebba, F., 1987. Foams and biliquid foams-aphrons. Wiley, Chichester.

Shivhare, S., Kuru, E., 2014. A study of the pore-blocking ability and formation damage characteristics of oil-based colloidal gas aphron drilling fluids. J. Pet. Sci. Eng. 122, 257–265. https://doi.org/10.1016/j.petrol.2014.07.018

Tabzar, A., Arabloo, M., Ghazanfari, M.H., 2015. Rheology, stability and filtration characteristics of Colloidal Gas Aphron fluids: Role of surfactant and polymer type. J. Nat. Gas Sci. Eng. 26, 895–906. https://doi.org/10.1016/j.jngse.2015.07.014

570 Telmadarreie, A., Doda, A., Trivedi, J.J., Kuru, E., Choi, P., 2016. CO2microbubbles - A potential
571 fluid for enhanced oil recovery: Bulk and porous media studies. J. Pet. Sci. Eng. 138, 160–
572 173. https://doi.org/10.1016/j.petrol.2015.10.035

573 Vo Thanh, H., Lee, K.-K., 2021. Application of machine learning to predict CO2 trapping
574 performance in deep saline aquifers. Energy 122457.
575 https://doi.org/10.1016/j.energy.2021.122457

576 Vo Thanh, H., Sugai, Y., Nguele, R., Sasaki, K., 2020a. Robust optimization of CO2 sequestration
577 through a water alternating gas process under geological uncertainties in Cuu Long Basin,
578 Vietnam. J. Nat. Gas Sci. Eng. 76, 103208. https://doi.org/10.1016/j.jngse.2020.103208

579 Vo Thanh, H., Sugai, Y., Nguele, R., Sasaki, K., 2019. Integrated workflow in 3D geological
580 model construction for evaluation of CO2 storage capacity of a fractured basement reservoir
581 in Cuu Long Basin, Vietnam. Int. J. Greenh. Gas Control 90, 102826.
582 https://doi.org/10.1016/j.ijggc.2019.102826

583 Vo Thanh, H., Sugai, Y., Sasaki, K., 2020b. Application of artificial neural network for predicting
584 the performance of CO2 enhanced oil recovery and storage in residual oil zones. Sci. Rep. 10,
585 1–16. https://doi.org/10.1038/s41598-020-73931-2

586 Wang, Y.D., Wen, H.Z., Huang, Y.Y., Dai, Y.Y., 2001. Separation of Cu(II) from an aqueous
587 solution by using colloidal gas aphrons. J. Chem. Eng. Japan 34, 1127–1130.
588 https://doi.org/10.1252/jcej.34.1127

589 Waters, K.E., Hadler, K., Cilliers, J.J., 2008. The flotation of fine particles using charged
590 microbubbles. Miner. Eng. 21, 918–923. https://doi.org/10.1016/j.mineng.2008.04.011

591 Wright, R., 1933. Jamin Effect in Oil Production. Bull. Am. Assoc. Pet. Geol. 17, 1521–1525.

592 Yang, E., Fang, Y., Liu, Y., Li, Z., Wu, J., 2020. Research and application of microfoam selective
593 water plugging agent in shallow low-temperature reservoirs. J. Pet. Sci. Eng. 193, 107354.
594 https://doi.org/10.1016/j.petrol.2020.107354

595 Yang, J., Wang, X., Peng, X., Du, Z., Zeng, F., 2019. Experimental studies on CO2 foam
596 performance in the tight cores. J. Pet. Sci. Eng. 175, 1136–1149.
597 https://doi.org/10.1016/j.petrol.2019.01.029

598 Zhang, Y., Gao, M., You, Q., Fan, H., Li, W., Liu, Y., Fang, J., Zhao, G., Jin, Z., Dai, C., 2019.
599 Smart mobility control agent for enhanced oil recovery during CO2 flooding in ultra-low
600 permeability reservoirs. Fuel 241, 442–450. https://doi.org/10.1016/j.fuel.2018.12.069

601 Zhu, W., Zheng, X., Li, G., 2020. Micro-bubbles size, rheological and filtration characteristics of
602 Colloidal Gas Aphron (CGA) drilling fluids for high temperature well: Role of attapulgite. J.
603 Pet. Sci. Eng. 186. https://doi.org/10.1016/j.petrol.2019.106683

604